Eur. Phys. J. A **16**, 583–597 (2003)
DOI 10.1140/epja/i2002-10116-7

THE EUROPEAN PHYSICAL JOURNAL A

^{2}H(^{3}He, t)2p reaction at 2 GeV

B. Ramstein[1,a], C. Mosbacher[2], T. Hennino[1], W. Augustyniak[7], D. Bachelier[1†], H.G. Bohlen[3], J.L. Boyard[1], R. Dahl[4], C. Ellegaard[4], C. Gaarde[4†], J. Gosset[5], J.C. Jourdain[1], J.S. Larsen[4], M.C. Lemaire[5], D. L'Hôte[5], H.P. Morsch[3], M. Österlund[6,b], J. Poitou[5], P. Radvanyi[3], M. Roy-Stephan[1], T. Sams[3,4], M. Skousen[4], S. Tarlé-Rousteau[1], and P. Zupranski[1,3,7]

[1] Institut de Physique Nucléaire, IN2P3(CNRS), 91406 Orsay Cedex, France
[2] Institut für Kernphysik, Forschungszentrum Jülich GmbH, D-52425, Germany
[3] Laboratoire National Saturne, IN2P3(CNRS) and DSM(CEA), F-91191 Gif-sur-Yvette Cedex, France
[4] Niels Bohr Institute, University of Copenhagen, DK-2100 Copenhagen, Denmark
[5] DSM/Dapnia, CEA/Saclay, 91191 Gif-sur-Yvette Cedex, France
[6] Institute of Physics, University of Lund, S-223 62 Lund, Sweden
[7] Soltan Institute for Nuclear Studies, 00681 Warsaw, Poland

Received: 21 October 2002 /
Published online: 11 March 2003 – © Società Italiana di Fisica / Springer-Verlag 2003
Communicated by M. Garçon

Abstract. The exclusive ^{2}H(^{3}He, t)2p reaction has been studied at 2 GeV for energy transfers up to 500 MeV and triton angles up to 3.4°. The protons were measured in the large acceptance magnetic detector DIOGENE, in coincidence with the forward tritons detected in a dedicated magnetic arm. The energy transfer spectra extend well above the pion threshold. However, in the region of Δ excitation, the yield is less than 10% of the inclusive ^{2}H(^{3}He, t) cross-section, which indicates the small contribution of the ΔN $\rightarrow$ NN process. The angular distributions of the two protons in their center of mass have been analysed as a function of energy transfer and triton angle and a Legendre polynomial decomposition has been achieved. These data have been compared to a model based on a coupled-channel approach for describing the NN and NΔ systems.

PACS. 25.55.Kr Charge-exchange reactions – 14.20.Gk Baryon resonances with $S = 0$ – 24.10.Eq Coupled-channel and distorted-wave models

1 Introduction

Excitation and decay of the Δ-resonance in nuclei have been studied intensively at Laboratoire National Saturne using the (^{3}He, t) reaction at 2 GeV [1–7]. Other inclusive and exclusive charge exchange experiments and some polarisation measurements have also been performed at SATURNE, KEK, LAMPF, Gatchina or Dubna using (p, n) [8–11], (d, 2p) [12], (^{3}He, t) [13], (t, ^{3}He) [14] and heavy-ion reactions [15,16]. These charge exchange experiments have brought information on the Δ-N interaction complementary to the one extracted in pion- or photon-induced experiments. Such reactions involve indeed both a spin-longitudinal (pion-like) and a spin-transverse (ρ-meson-like or photon-like) excitation and investigate the nuclear response in the space-like region ($\omega < q$), while pion-induced reactions are purely longitudinal probes along the lines $\omega^2 - q^2 = m_\pi^2$ and photon-induced reactions purely transverse probes along the line $\omega = q$.

Theoretical models have been developed to describe the energy transfer spectra for the inclusive (^{3}He, t) and (p, n) reactions as well as for the different decay channels measured in the exclusive experiments [17–22]. In the Δ-hole model [21], the role of the spin-longitudinal and spin-transverse excitations has been studied in detail.

On the one hand, the longitudinal component extracted from the ^{12}C($\mathbf{p}, \mathbf{n}$) polarisation measurements in the Δ region [10] is fairly well reproduced by the model, and so is the coherent pion production measured in the exclusive experiments [5,21], which is mainly due to the longitudinal excitation. In the Δ-hole model, the nuclear response induced by this part of the interaction is found to be very sensitive to the attractive spin-longitudinal Δ-hole correlations, confirming earlier predictions [23,24].

[a] e-mail: ramstein@ipno.in2p3.fr
[b] *Present adress*: School of Engineering, Jönköping University, P.O. Box 1026, S-551 11 Jönköping, Sweden.
[†] Deceased.

On the other hand, the transverse component is underestimated by the model in the low-energy part of the resonance and in the dip region lying between the quasi-elastic peak and the Δ bump. An excess of transverse cross-section is also found in the quasi-elastic region for the ^{12}C(p, n) reaction [25], whereas a DWIA calculation with a $\pi + \rho + g'$ residual interaction is able to reproduce the longitudinal response. The role of 2p-2h correlations [26] and meson exchange currents [27] is advocated, but this excess of cross-section in the transverse channel is not yet quantitatively reproduced.

The deuterium target is a much simpler case where the roles of the Δ-N interaction and meson-exchange currents can be investigated alone and where more complete calculations are practicable. A theoretical calculation of the ^{2}H(p, n) reaction has been proposed by Ch. Mosbacher and F. Osterfeld [28] and then extended to ^{2}H(^{3}He, t) [29]. Based on a coupled-channel approach to describe the intermediate Δ-N or NN system in a non-relativistic framework, this model allows a calculation of the energy transfer spectra in the quasi-elastic, dip and Δ regions as well as in the different exit channels (πd, πNN, NN). An overall successful description of the total-energy transfer spectra measured at LAMPF in the ^{2}H(p, n) reaction [28] and at SATURNE in the ^{2}H(^{3}He, t) reaction [29] is obtained both in the quasi-elastic and Δ regions. However, like in the case of ^{12}C, the model fails to describe the dip region at the largest scattering angles and the low-energy side of the resonance. From the comparison with the $^2\mathbf{H}(\mathbf{p},\mathbf{n})$ polarisation measurements [30], the discrepancy in the dip region could be again assigned to the transverse component. This was interpreted by the authors as an effect of two-body meson-exchange currents and related to the significant effect of such processes in (e,e$'$) reactions [31]. On the low-energy side of the resonance, the discrepancy is attributed to Δ excitation in the projectile. A long time ago, E. Oset *et al.* developed a quite different model including both excitation of the Δ-resonance in the projectile and in the target [17,32] and were able to reproduce rather well the ^{2}H(^{3}He, t) energy transfer spectrum at 0°. The contribution of Δ excitation in the projectile was about 30% of the total and the contribution of target excitation was much smaller than in the model by Mosbacher *et al.*

Exclusive ^{2}H(^{3}He, t)2p data can be useful in this context. First, if a Δ is excited in the projectile and a triton is detected, the energy has to be carried by a pion, so this process is not contributing in the ^{2}H(^{3}He, t)2p reaction. In this reaction, the spin-longitudinal and spin-transverse excitations are not separated. However, the angular distributions of the protons might be sensitive to the spin structure of the excitation and the comparison to the coupled-channel model may shed some light on the origin of the discrepancy observed in the transverse channel. Above the pion threshold, where the Δ-resonance dominates the inclusive cross-section, the ^{2}H(^{3}He, t)2p data are expected to give direct information on the ΔN $\rightarrow$ NN transition. This transition is of high interest for the understanding of the behaviour of Δ's in nuclear matter, since it is the dominant decay channel at small energy transfers [5,6]. The ^{2}H(^{3}He, t)2p data can therefore serve as a testing bench for calculations of the decay modes of the Δ-resonance in nuclei. Previously, the p(d, pp)n reaction had been studied at 1 GeV at Dubna in a bubble chamber experiment. A contribution from the Δ-resonance had been clearly identified and its yield was found in agreement with calculations in the one-pion exchange approximation [33,34], but the statistics was too low to study the proton angular distributions in the Δ-resonance region.

In this paper, the data obtained for the ^{2}H(^{3}He, t)2p reaction at 2 GeV measured at Laboratoire National Saturne with the DIOGENE detector are presented and compared with the predictions of the coupled-channel model. Section 2 is devoted to the description of the experimental conditions and sect. 3 to the details of the data analysis. In sect. 4, we discuss the experimental results. The ingredients of the model, its results and the comparison to the data are presented in sect. 5.

2 Experimental conditions

2.1 Experimental set-up

The 2 GeV incident energy ^{3}He beam was provided by the MIMAS-SATURNE accelerators of the Laboratoire National Saturne at Saclay. The experimental set-up (fig. 1) consisted of a liquid-deuterium target and two main detection components: a large acceptance detector (DIOGENE) located around the target, detecting pions and protons produced in the reaction and a magnetic dipole (CHALUT) analysing forward emitted tritons. The acquisition system was triggered by the detection of a triton.

The liquid ^{2}H target was a 20 cm long and 5.4 cm in diameter cylinder with mylar walls, a titanium back window and a mylar front window, 120 μm, 28 μm and 120 μm thick, respectively [35]. Pipes used to fill and empty the target with liquid ^{2}H were inserted in a 3 cm wide and 12 mm thick copper ring surrounding the target and centered 3 cm downstream from the back window. The target center was located 20 cm upstream from the DIOGENE center, in order to improve the acceptance at small angles.

DIOGENE was a pictorial drift chamber consisting of a 80 cm long barrel housing 10 trapezoidal drift chambers arranged around the beam pipe. The whole assembly was put in a 1.0 T longitudinal magnetic field. A complete description of the DIOGENE detector can be found in ref. [36]. We concentrate here only on the main features. In each drift chamber, 16 resistive anode wires parallel to the beam axis were used to measure the drift times and the charges collected at both ends of the wires. Particle identification and momentum vector reconstruction were then achieved with the data analysis program RATRADI [36] modified for extended targets [37]. A $2\cdot10^5$/s incident particle rate was chosen to limit space charge effects in the drift cells.

The triton detection arm consisted of the magnetic dipole analyser CHALUT operated at 1.9 T, and two identical four-layer drift chambers CH1 and CH2, followed

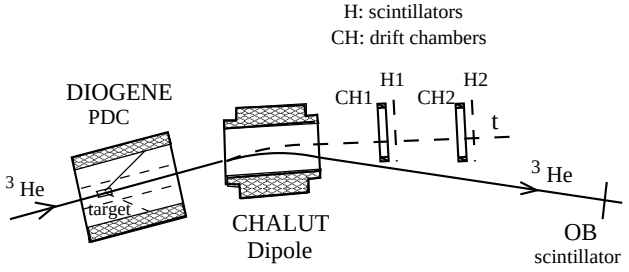

Fig. 1. Experimental set-up.

by scintillator hodoscopes H1 and H2, respectively. The H1 and H2 hodoscopes consisted of twelve scintillators, 2 mm and 10 mm thick, respectively. A coincidence between corresponding scintillators of each plane triggered the electronics. This condition and the geometry of the hodoscope were accurately tuned in order to select particles with p/Z larger than 3.1 GeV/c, which corresponded for the (^{3}He, t) reaction to energy transfers lower than 600 MeV. The rejection of low-momentum particles was necessary due to the high number of deuterons coming from the ^{3}He beam break-up on the target, with a very broad momentum distribution peaked at two thirds of the beam momentum (*i.e.* 2.6 GeV/c). The ^{3}He beam was directed through a vacuum pipe to a beam dump located at the farthest downstream end of the spectrometer. Two helium bags were inserted between the magnet and the first chamber and between the two chambers in order to reduce multiple scattering.

2.2 Acceptance and resolutions

In order to ensure good resolution on the track reconstruction and good discrimination of pions and protons emitted from any point of the target, the polar angle range was restricted to the interval [20°, 132°]. The energy loss of the protons in the target and carbon fiber beam pipe set an angle-dependent energy threshold. It had a minimum value of 29 MeV for particles emitted at 90° and reached 33 MeV at 130° and 52 MeV at 20°.

Momentum resolution (FWHM) for the protons in the DIOGENE detector was 20% on average; polar and azimuthal angles were measured with a precision of about 4.5°. Multiple scattering in the gas was the main contribution to the error on proton momenta and polar angles, for proton momenta lower than 500 MeV/c. Above this value, the uncertainty due to the determination of the transverse (respectively, longitudinal) coordinates became important for the determination of the errors on the momentum (respectively, polar angles), especially at forward and backward angles where fewer wires were hit. Eventually, the error on the azimuthal angle was dominated by the multiple scattering in the target and in the 2 mm thick carbon fiber vacuum tube. The intersection point between the track and the beam axis was determined with a 2 cm (FWHM) longitudinal accuracy. Due to the thick copper rings around the backward part of the target, the detection efficiency for protons produced in the first seven centimeters of the target was very low. This part of the target was therefore excluded in the analysis.

Tritons with kinetic energies above 1.45 GeV and angles smaller than 3.4° were measured in the forward detection arm. The height of the first drift chamber CH1 induced a cut in the vertical plane, which could be well approximated by a sharp window [−14, +14 mrad]. In the horizontal plane, the angular opening was about [−10, +60 mrad] due to the entrance and exit windows of the CHALUT magnet.

The incoming beam angular apertures, about 4.7 mrad (FWHM) in both horizontal and vertical planes, were the dominant contribution to the error on the triton angle. The error on the triton energy was mainly due to the beam extension in the horizontal plane (FWHM = 6 mm) and amounted to 40 MeV at 0°. An additional error roughly proportional to the horizontal angle was due to the uncertainty on the vertex position along the beam direction and led to a total error of about 60 MeV at 3.4°. When a particle was detected in DIOGENE, however, the interaction point was defined with a precision along the beam direction of about 2 cm (FWHM), which allowed to correct the triton energy with enough accuracy to keep the 40 MeV resolution up to 3.4°.

The counting rate measured in the OB scintillator located at the end of the beam line provided a normalisation of the cross-sections with a precision of 25%. The cross-sections were fully consistent in the whole angular range with the inclusive measurements performed at SPES4 [29] which were then used to get an absolute normalisation with a 15% precision.

Due to the 3 μs wide acquisition gate, the probability of recording a triton and one or two uncorrelated protons was about 30% on average, but most of these events were rejected because of their unphysical drift times in the DIOGENE cells, so that their contribution to the reconstructed events is not more than a few percent on average.

3 Data analysis

The inclusive ^{2}H(^{3}He, t) reaction at 2 GeV consists of four main partial channels:

$$^3\mathrm{He} + ^2\mathrm{H} \rightarrow \mathrm{t} + ^2\mathrm{H} + \pi^+ , \quad (1)$$

$$\rightarrow \mathrm{t} + 2\mathrm{p} , \quad (2)$$

$$\rightarrow \mathrm{t} + 2\mathrm{p} + \pi^0 , \quad (3)$$

$$\rightarrow \mathrm{t} + \mathrm{p} + \mathrm{n} + \pi^+ . \quad (4)$$

Both π^+ and protons were measured in the present experiment. However, as this paper concerns mainly the ^{2}H(^{3}He, t)2p process, we will only consider events with no pion emitted and compare their yield to the ^{2}H(^{3}He, t) inclusive reaction.

3.1 Inclusive ^{2}H(^{3}He, t) process

Investigation of the inclusive ^{2}H(^{3}He, t) process is achieved using events corresponding to a triton detected

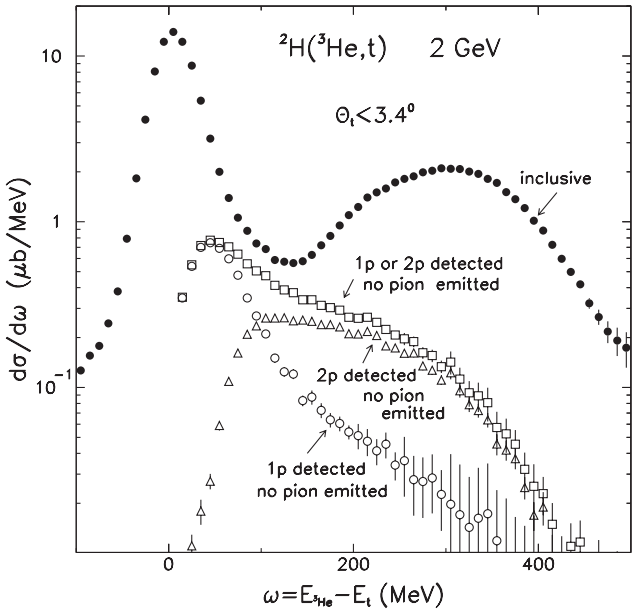

Fig. 2. Energy transfer spectra measured in the experiment: without any condition on the particles detected in DIOGENE (full circles), in the case of one proton detected and no pion emitted (open circles), in the case of two protons detected and no pion emitted (open triangles), in any of these two cases (open squares).

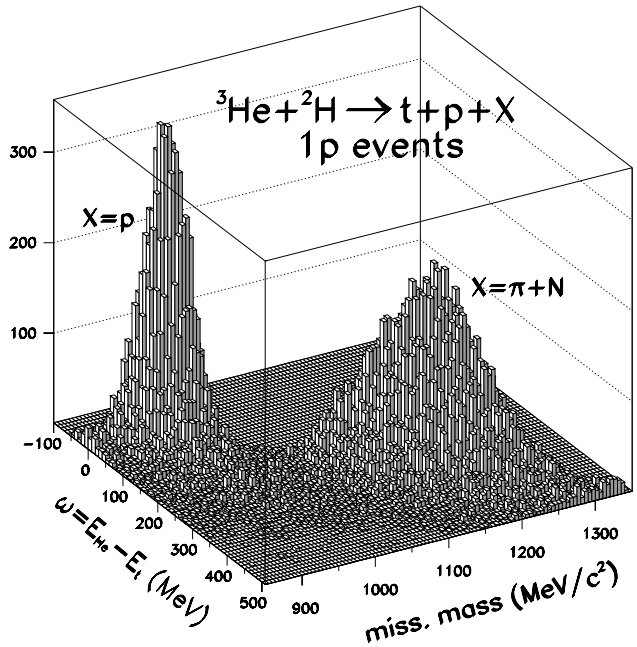

Fig. 3. The missing mass is plotted as a function of the energy transfer when only one proton was detected in coincidence with the triton.

in the forward detection arm, without any condition on detection of particles in DIOGENE. The energy transfer spectra obtained for these events are plotted as full circles in fig. 2. The yields are corrected on an event by event basis for the cut in the vertical angles of the tritons. This correction factor varies from 1 for angles smaller than 0.6° degrees to 13 at 3.4°. The uncertainty on this correction, due to the resolution in the triton angle, is included in the error bars.

Most of the deuterons coming from the ^{3}He break-up were rejected by the trigger, due to their low momenta, as explained in sect. 2. Their momentum distribution extends however up to 3.39 GeV/c, which is the kinematic limit for the reaction ^{2}H(^{3}He, d)^{3}He and corresponds to energy transfers for the (^{3}He, t) reaction of about 400 MeV. This contribution can be subtracted using the spectrum of the SPES4 inclusive measurements [29], where the deuterons were rejected by a time-of-flight measurement. The contribution amounts to 50% at 500 MeV; it then decreases rapidly and cancels at 400 MeV. The subtraction of these deuterons induces large error bars on the data points at the highest energy transfers (fig. 2).

The contribution of the empty target, due mainly to the titanium windows of the liquid target was about 1.5% on average.

In [29], we had presented inclusive 2 GeV ^{2}H(^{3}He, t) data at 0.25°, 1.6°, 2.7° and 4.0° obtained at SATURNE with the high-resolution SPES4 spectrometer. We carefully checked that the present data were compatible with the previous ones, when resolution effects and triton energy calibration precision were taken into account.

3.2 Exclusive ^{2}H(^{3}He, t)2p process

3.2.1 Selection of the process

Using the kinematical constraints of the ^{2}H(^{3}He, t)2p reaction, events with two protons (2p) or one proton (1p) detected in the DIOGENE detector can both be used to investigate the ^{2}H(^{3}He, t)2p reaction.

In the case of 1p events, the missing mass of the reaction ^{2}H(^{3}He, t)p allows a separation between events coming from reaction (2), where only one proton is missed by the detector, and events coming from reactions (3) and (4), where both one nucleon and one pion are missing. This is illustrated in fig. 3, where the 1p events missing mass is plotted as a function of the energy transfer. The events are located in two distinct regions: the peak at missing masses around the proton mass (reaction (2)) and the broad structure located at missing masses larger than the sum of the nucleon and pion masses (reactions (3) and (4)). Due to the pion emission threshold, only the first group of events is present at small energy transfers. Its contribution decreases rapidly with increasing energy transfer and above 200 MeV, events with one pion emitted dominate. For the present analysis, we kept only the first group of events, by selecting missing masses between 800 and 1025 MeV/c^2. The lower limit allows the rejection of chance coincidences between a triton and a proton.

When two protons p_1 and p_2 are detected in DIOGENE, we calculate the missing masses MM_1 and MM_2 corresponding to the reactions ^{2}H(^{3}He, t)p_1 and ^{2}H(^{3}He, t)p_2 (fig. 4). The two quantities are very well correlated and distributed around the proton mass as expected from reaction (2). A very small contribution of events with one

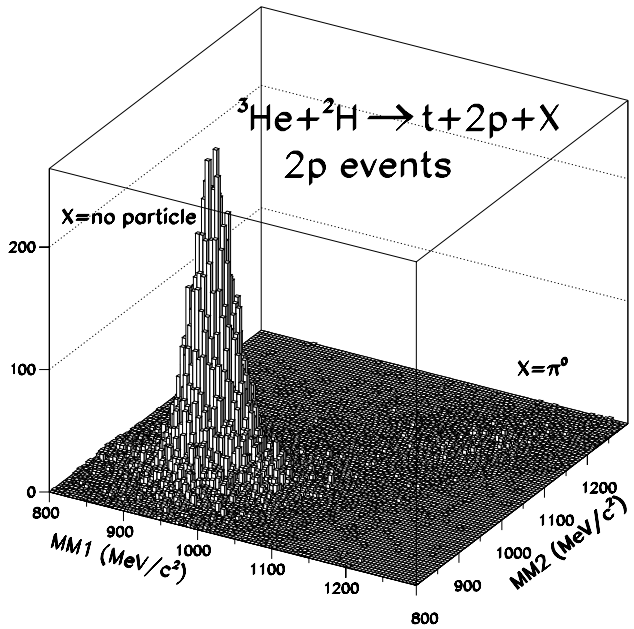

Fig. 4. When two protons are detected, the missing mass of the reaction ^{2}H(^{3}He, t)pX calculated with one proton is plotted as a function of the missing mass calculated with the other one.

pion missing, *i.e.* arising from reaction (3), can be observed. It amounts to about 2% of the total 2p yield. To reject this contribution and limit the chance coincidences, we put gates both on these two missing masses and on the one calculated for the reaction ^{2}H(^{3}He, t)2p.

The residual chance coincidence rate is of the same order for the two types of events. It is very small for energy transfers smaller than 250 MeV. Above this value, this contribution becomes significant at small angles, it stays however smaller than the error bars on each plot presented in this paper.

For a small fraction of the 1p events fullfilling the missing-masses constraints, the missing proton had momentum and angle above the detector cuts and, therefore, should have been detected. By normalizing to the number of events where the proton was detected, the inefficiency of the proton detection could be calculated as a function of angle and momentum. The inefficiency for proton detection in this experiment was found to be less than 6% in average, resulting from a 3% inefficiency for the central part of the acceptance and higher values at forward and backward angles. This inefficiency is most probably due to the small dead zones between the neighboring sectors, which affects the reconstruction of the tracks when few wires are hit.

The contribution from the target windows was eliminated by a cut on the interaction vertex. The correction for the triton acceptance was made as explained above (see subsect. 3.1).

3.2.2 Energy transfer spectra

The spectra obtained for the selected 1p and 2p events and for their sum are plotted as open circles, open triangles and open squares respectively, in fig. 2 . The error bars include statistical errors, uncertainties in the triton acceptance correction and errors in the selection of the ^{2}H(^{3}He, t) 2p process. At large energy transfers, the main contribution to the errors is due to the rejection of events with one pion emitted.

Due to the high-energy threshold of the DIOGENE detector, 1p events are very useful to obtain information on the lowest energy transfers. Above 100 MeV, the probability of detecting both emitted protons rapidly increases. However, up to 250 MeV, 1p events are still useful to extend the range of center-of-mass angles accessible in the experiment, which is important for the analysis of the angular distributions as will be seen later.

3.2.3 Angular distributions in the 2p center of mass

In the ^{2}H(^{3}He, t)2p reaction, the two-proton center of mass has a velocity:

$$\boldsymbol{\beta} = \mathbf{q}/(\omega + M_{\mathrm{d}})$$

where $\mathbf{q}$ and ω are, respectively, the momentum and energy transfers and M_{d} is the deuteron mass.

We then define in this two-proton center-of-mass frame the polar angle θ^*_{p} of the proton with respect to the $\mathbf{q}$-direction. The corresponding angular distributions $\frac{\mathrm{d}\sigma}{\mathrm{d}\Omega^*_{\mathrm{p}}}$ measured for protons detected in our experiment are plotted in fig. 5 for different energy transfer and triton angle bins. When both protons are detected, we plot the angles calculated from the measurements of each of them. The two protons are emitted back to back in their center of mass, that means with polar angles symmetric with respect to 90°. Due to resolution effects, the correlation is however broadened and has a width of about 4° (FWHM).

When only one proton is detected, the angle calculated for the missing proton is also plotted, in order to avoid introducing a false asymmetry.

The errors on the data points are due to statistics, correction for triton acceptance and identification of the ^{2}H(^{3}He, t)2p process. For the largest energy transfer bin (ω = 300–350 MeV), only 2p events were considered since the 1p events induce larger relative error bars (cf. fig. 2).

3.2.4 Acceptance corrections

As described in section 2.2, the experimental set-up presents a dead zone at forward and backward angles, as well as an energy threshold which varies with the proton angle. As these cuts apply in the laboratory system, the distortions induced on the center-of-mass angular distributions are heavily dependent on triton angle and energy transfer.

A Monte Carlo simulation of the ^{2}H(^{3}He, t)2p reaction including the effects of resolution, acceptance and efficiency of the experimental set-up (see subsect. 2.2) was developed to quantify these experimental effects.

The protons were generated in the simulation with an isotropic ϕ^*_{p} distribution, which is justified by the fact that

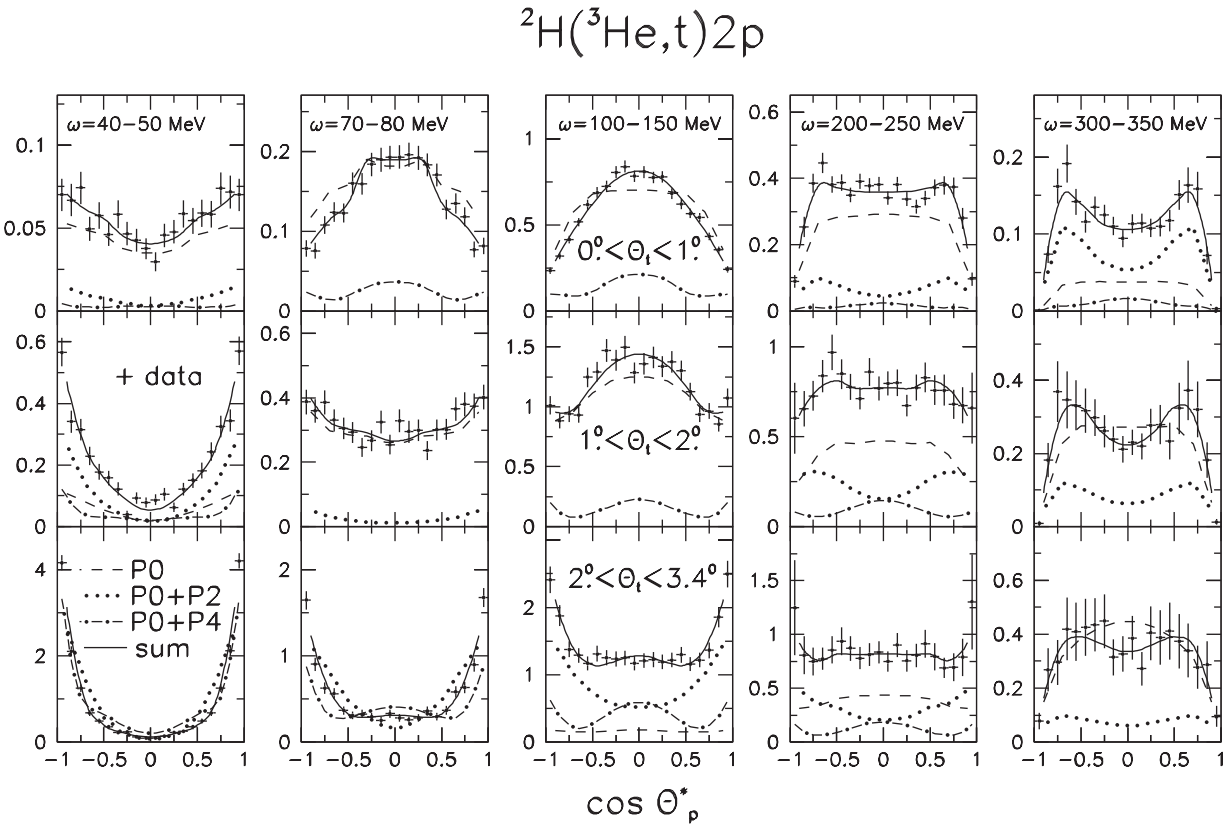

Fig. 5. Measured angular distributions of the two protons in their center of mass. Each row corresponds to a given triton angle bin and each column to a given energy transfer bin, as indicated. Acceptance corrected angular distributions will be shown in fig. 10 below. The full line is the result of a fit by a linear combination of three simulated distributions resulting from Legendre polynomials P_0, P_2 and P_4 modified by experimental resolution and acceptance (see text). The contributions of P_0 (dashed line), $P_0 + P_2$ (dotted lines) and $P_0 + P_4$ (dash-dotted line) are also shown, when they are positive.

no anisotropy was found in the experimental $\phi^*_{\rm p}$ distributions in all the phase space regions where it could be investigated.

In fig. 6, the efficiencies calculated with the simulations and averaged over several energy transfer and triton angle bins are plotted as a function of the proton angles. For energy transfers of 40–50 MeV (first column of fig. 6), the acceptance is significant only for triton angles larger than about 2°, where both the forward emitted protons are the most energetic and the angle of the momentum transfer is well above the angular cut of the detector so that they fall inside the acceptance of the detector. At smaller triton angles, the acceptance in this energy transfer bin is only due to higher initial energy transfers shifted towards lower values due to the resolution.

When increasing the energy transfer well above the energy threshold for proton detection (2nd to 4th column of fig. 6), the acceptance gets much higher. At triton angles below 1°, as the angle of the momentum vector points into or close to the forward angular cuts of the detector, protons emitted forwards or backwards with respect to **q** have a small probability to be detected. At larger triton angles, due to the angle of **q**, also central $\theta^*_{\rm p}$ are cut by the acceptance. Full acceptance at 90° is achieved for the largest triton angle bin only for energy transfers higher than 150 MeV (4th column of fig. 6), where the angle of the momentum vector is small enough. The acceptance is then cut only at forward and backward angles, like in the case of small triton angles, but in a less sharp way and in a broader region.

3.2.5 Legendre polynomial decomposition of the proton angular distributions

In order to obtain a quantitative and acceptance independent description of the experimental angular distributions, Legendre polynomial decomposition was applied. For this purpose, we used the Monte Carlo simulation program of the experimental set-up and generated three sets of events where the angular distributions of the protons followed three different positively defined combinations of the three first Legendre polynomials:

$$P_0(\cos\theta^*_{\rm p}) = 1$$

$$P_0(\cos\theta^*_{\rm p}) + P_2(\cos\theta^*_{\rm p}) = (1 + 3\cos^2\theta^*_{\rm p})/2$$

and

$$P_0(\cos\theta^*_{\rm p}) + P_4(\cos\theta^*_{\rm p}) = (35\cos^4\theta^*_{\rm p} - 30\cos^2\theta^*_{\rm p} + 11)/8\,.$$

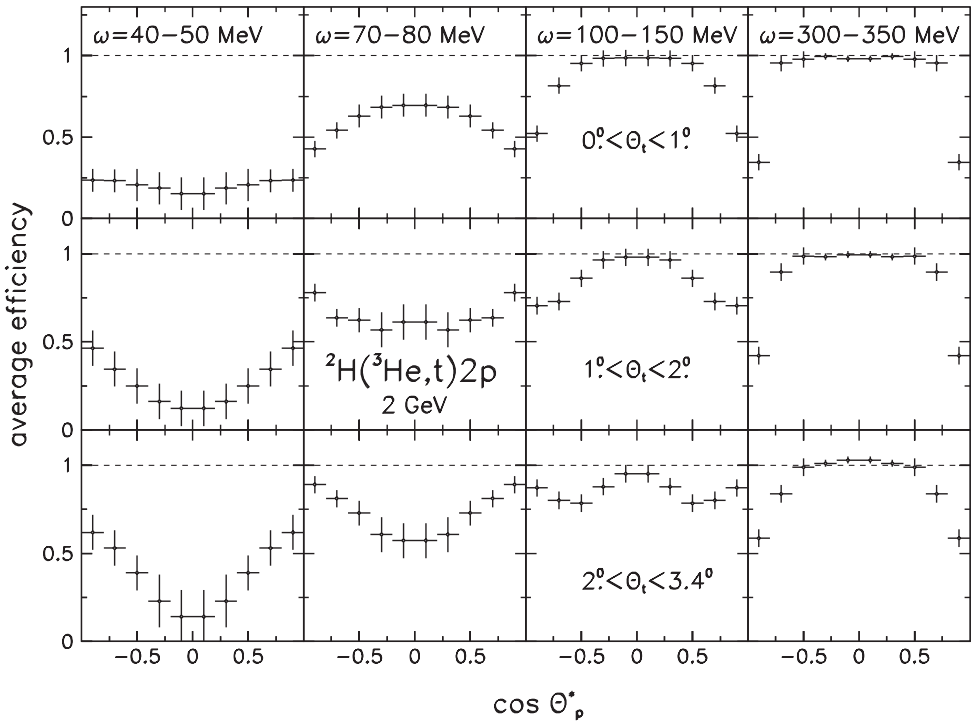

Fig. 6. The average efficiency for the detection of one of the two protons emitted in the reaction ^{2}H(^{3}He, t)2p is plotted as a function of $\cos\theta_{\rm p}^*$ for different bins in triton angle and energy transfer.

The distributions of protons obtained after the filter of the detection are then used to fit the experimental data and to extract the parameters A_0, A_2 and A_4 of the decomposition

$$\frac{{\rm d}^3\sigma}{{\rm d}\Omega_{\rm t}{\rm d}\omega{\rm d}\Omega_{\rm p}^*}(\theta_{\rm t},\omega,\cos\theta_{\rm p}^*)=\frac{1}{4\pi}\sum_{i=0}^{2}A_{2i}(\theta_{\rm t},\omega)P_{2i}(\cos\theta_{\rm p}^*).$$

As the integral of $P_{2i}(\cos\theta_{\rm p}^*)$ over $\cos\theta_{\rm p}^*$ is 2.0 for $i=0$ and 0.0 for the other values of i, $A_0(\theta_{\rm t},\omega)=\frac{{\rm d}^2\sigma}{{\rm d}\Omega_{\rm t}{\rm d}\omega}(\theta_{\rm t},\omega)$ measures the ^{2}H(^{3}He, t) cross-section, whereas the ratios A_2/A_0 and A_4/A_0 give information on the shape of the two-proton angular distributions in their center of mass.

For the lowest energy transfers (below 70 MeV), the tritons have been generated with distributions given by the calculation of [29] which has been shown to reproduce the inclusive spectrum rather well. It is indeed necessary to have a dependence of the cross-sections close to reality, since the acceptance corrections vary quite rapidly as a function of energy transfer. Above 70 MeV, the dependence is smoother and the tritons have been generated uniformly as a function of energy transfer and angle.

The fitting procedure is performed independently in 36 cells corresponding to different energy transfer and triton angle windows: the triton angular range has been divided into the three following bins [0°-1°], [1°-2°] and [2°-3.4°] and the energy transfer range was cut into six 10 MeV bins from 40 to 100 MeV and six 50 MeV bins from 100 to 400 MeV.

Some examples of the quality of the fits and of the respective weights of the three Legendre polynomial combinations are shown in fig. 5, while the values of the parameters extracted from the analysis are plotted in fig. 7, fig. 8 and fig. 9.

As already stressed, the A_0 parameter stands for the ^{2}H(^{3}He, t)2p cross-section in the corresponding energy transfer and triton angle range and is compared to the inclusive cross-section in fig. 7.

Below the pion threshold, the ^{2}H(^{3}He, t)2p cross-sections extracted from the analysis of the angular distributions are in good agreement with the inclusive cross-sections (fig. 7), as it should be since no other channel is open. This is a good check of the procedure and confirms the validity of the parameters extracted at larger energy transfers, all the more since the acceptance corrections are smaller there.

Below 70 MeV, the acceptance correction factors are very large (fig. 6) and vary rapidly with the energy transfer. The extracted ^{2}H(^{3}He, t)2p cross-sections are therefore very sensitive to small uncertainties in the geometry of the detection or triton energy calibration and can be determined only within a factor up to 2. These values are not shown in the picture for the sake of clarity, but are still compatible with the inclusive ^{2}H(^{3}He, t) cross-sections. For both inclusive and 2p channels, the values obtained result from the convolution of the sharp initial energy transfer dependence with the energy resolution of the experimental set-up (about 40 MeV FWHM on average). This has an important effect on the width of the low energy peak. Above 70 MeV, the distortion of the spectra is small due to the quite smooth slope of the cross-section.

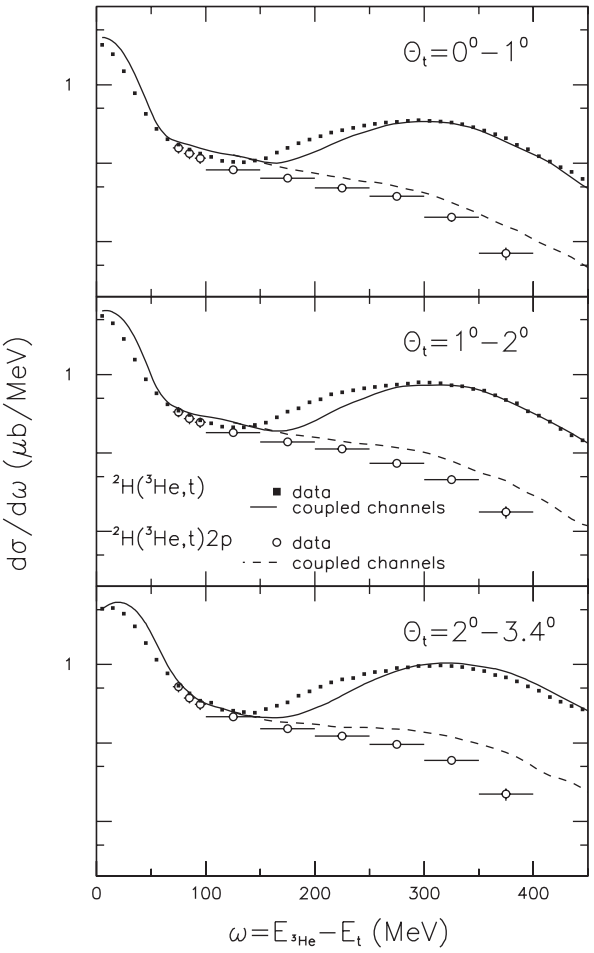

Fig. 7. Acceptance corrected differential cross-sections obtained for the ^{2}H(^{3}He, t)2p reaction (open circles) and inclusive ^{2}H(^{3}He, t) yields (full squares) are compared to the predictions of the coupled-channel model (repectively full and dashed lines).

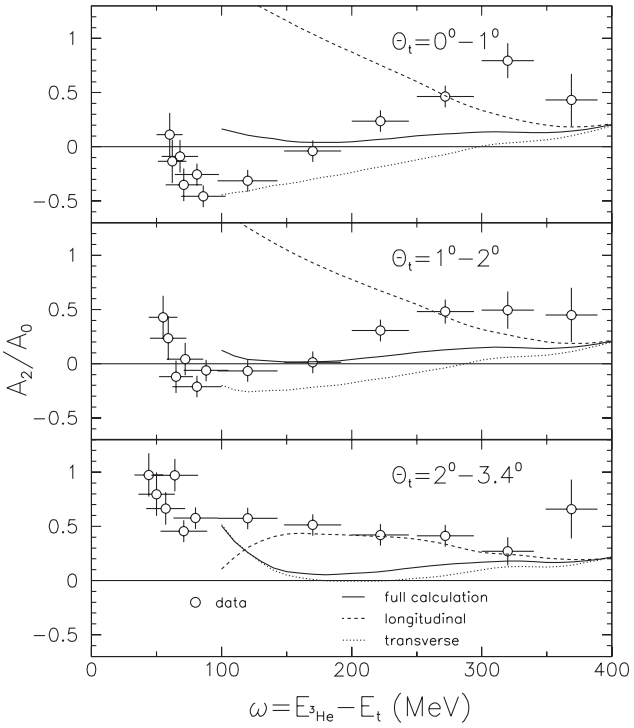

Fig. 8. Ratio of the A_2 and A_0 parameters obtained by the decomposition of the two-proton angular distributions in Legendre polynomials (open circles). The energy transfers and horizontal bars correspond respectively to the mean values and rms of the distributions of energy transfers over which the results are averaged. The lines show the predictions of the coupled-channel model: full calculation (full line), longitudinal interaction only (dashed line) and transverse interaction only (dotted line).

The A_2/A_0 and A_4/A_0 parameters are displayed in fig. 8 and fig. 9 as a function of energy transfer. To correct for resolution effects, the distributions of initial energy transfers have been calculated for each bin, using the simulation taking into account all experimental effects. The energies and horizontal bars reported on the figure correspond respectively to the mean values and rms of these distributions.

The fit by a $(A_0 \cdot P_0 + A_2 \cdot P_2 + A_4 \cdot P_4)$ combination gives a satisfactory result for each bin (see fig. 5). The error bars in fig. 8 and fig. 9 take into account statistics, fit accuracy and acceptance correction uncertainties. For energy transfers lower than 70 MeV, information on the A_2/A_0 and A_4/A_0 parameters could be obtained, despite the high uncertainty on the acceptance corrections. However, a significant contribution of P_6 Legendre polynomial is not excluded, especially at large triton angles.

The acceptance correction factors deduced from the simulation (fig. 6) have been used to correct the angular distributions, as shown for some examples in fig. 10. Below

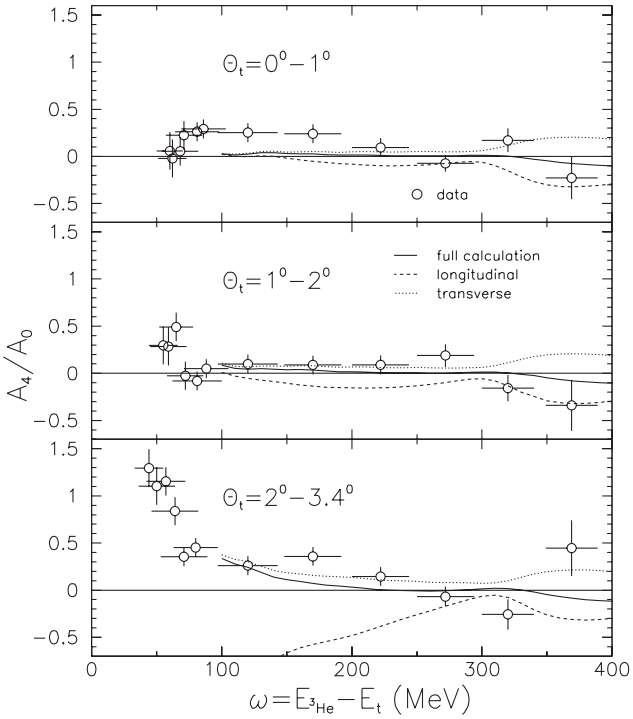

Fig. 9. Same as fig. 8 for the A_4/A_0 ratio.

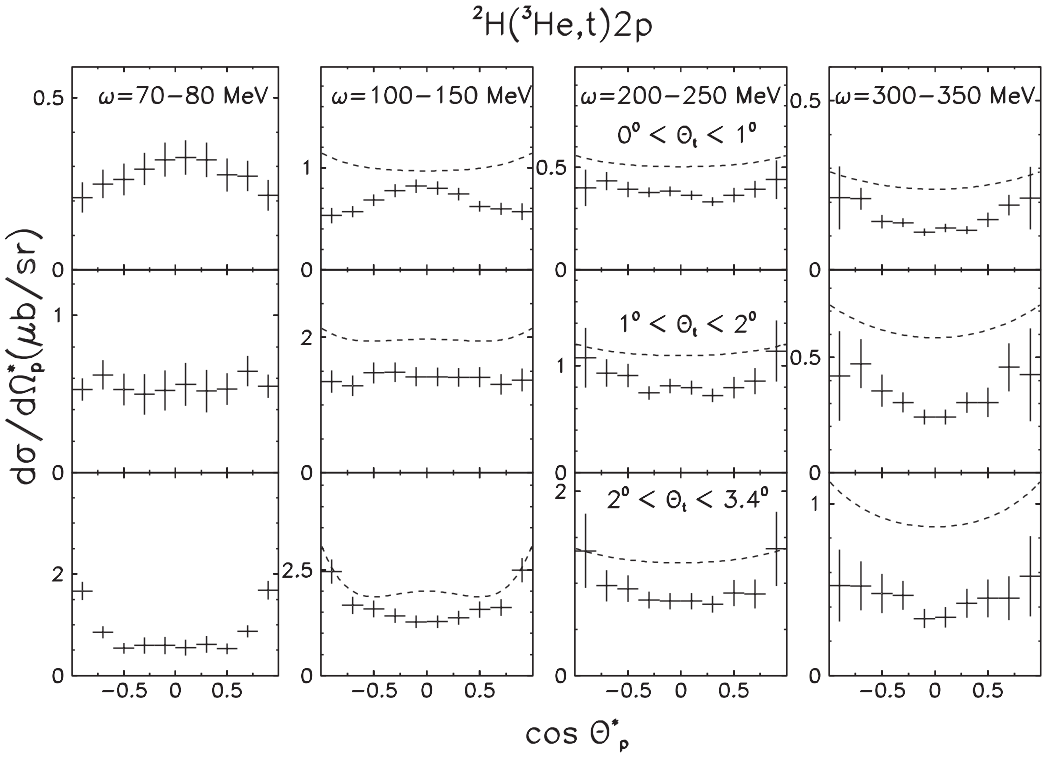

Fig. 10. Acceptance corrected angular distributions of the two protons in their center of mass are compared to the predictions of the coupled-channel model (dashed line).

70 MeV, the errors on the acceptance factor are too large to allow for such corrections.

A first analysis of the 2p angular distributions had been performed previously for a restricted zone of the acceptance using a $A_0 \cdot P_0 + A_2 \cdot P_2$ fit [38]. The A_0/A_2 obtained this way had larger error bars but were compatible with the present ones in the Δ-resonance region, where the P_4 contribution is small.

4 Experimental results

As already mentioned, the inclusive ^{2}H(^{3}He, t) experiment has been studied at 2 GeV in the same angular range with a much better energy resolution [29]. The present inclusive data are however very helpful because they allow a direct comparison to the ^{2}H(^{3}He, t)2p data in the same experimental conditions. We will therefore present the features of our inclusive data which are relevant for this comparison.

As in all charge exchange reactions in this energy regime [39,16], the inclusive spectrum exhibits two well-defined structures. The first one appears as a rather narrow peak at small energy transfers and corresponds to quasi-elastic mechanisms involving only nucleonic degrees of freedom. The second one is a broad bump showing up above the pion threshold and corresponds to the excitation of a nucleon into a Δ-resonance. The angular distributions in the quasi-elastic and Δ-resonance regions have been shown in ref. [29]. Here, we present the inclusive yields after integration over three triton angle bins.

The dependence of the ^{2}H(^{3}He, t)2p cross-section as a function of energy transfer has a very sharp slope at low energy transfers, it then flattens, but no structure is seen in the region of the Δ-resonance. In addition, the comparison with the inclusive cross-section leads to the important conclusion that the Δ excited in the ^{2}H(^{3}He, t) reaction has a weak branching ratio towards the ΔN $\rightarrow$ pp process (fig. 7).

The shape of the 2p angular distributions in their center of mass has a clear dependence on triton angle and energy transfer (fig. 10). This evolution is seen more quantitatively in fig. 8 and fig. 9, where the A_2/A_0 and A_4/A_0 ratios extracted from the fit of the experimental angular distributions are presented, respectively (see subsubsect. 3.2.3).

These differential cross-sections result from the excitation process (quasi-elastic process or excitation of a Δ-resonance) and from the NN $\rightarrow$ NN final-state interaction or NΔ $\rightarrow$ NN transition.

In the following, we will compare the cross-sections and the shapes of the angular distributions obtained from our analysis with the theoretical model of ref. [28] in order to extract information on the ^{2}H(^{3}He, t)2p transition process and on the spin structure of the excitation.

5 Theory

In ref. [29], the high-precision 2 GeV ^{2}H(^{3}He, t) inclusive data had been compared to theoretical predictions by

Ch. Mosbacher *et al.* This calculation, first developed for the (p, n) charge exchange reaction [28] , includes both quasi-elastic and Δ excitation processes.

As the model is also able to describe the different exclusive channels following Δ excitation, we compare its predictions to the present ^{2}H(^{3}He, t)2p energy transfer spectra and angular distributions.

5.1 Description of the model

The original model and the modifications applied to treat the (^{3}He, t) case have been described in ref. [28] and ref. [29], respectively. For the sake of consistency, we recall here only of the basic features of the model.

The model is based on a modification of the Δ-hole model of Osterfeld *et al.* [18], for the 2-body deuterium system, so that the correlated wave functions of the NN or ΔN intermediate system are calculated by solving a coupled equation system. The method allows to take into account the Δ-N interaction and the NN final-state interaction to any order.

The quasi-elastic process and the Δ excitation in deuterium are treated using the following effective parameterizations of the NN $\rightarrow$ NN and NN $\rightarrow$ ΔN transition matrices for the interaction of the projectile nucleon i with target nucleon j:

$$t_{\mathrm{NN,NN}} = (\alpha(\boldsymbol{\sigma_i}\cdot\mathbf{q})(\boldsymbol{\sigma_j}\cdot\mathbf{q}) + \beta(\boldsymbol{\sigma_i}\times\mathbf{q})(\boldsymbol{\sigma_j}\times\mathbf{q}))\boldsymbol{\tau_i}\cdot\boldsymbol{\tau_j}$$

and

$$t_{\mathrm{NN,N\Delta}} = (\gamma_{\mathrm{lo}}(\boldsymbol{\sigma_i}\cdot\mathbf{q})(\mathbf{S}_j^\dagger\cdot\mathbf{q}) + \gamma_{\mathrm{tr}}(\boldsymbol{\sigma_i}\times\mathbf{q})(\mathbf{S}_j^\dagger\times\mathbf{q}))\boldsymbol{\tau_i}\cdot\mathbf{T}_j^\dagger,$$

where $\boldsymbol{\sigma}$ and $\boldsymbol{\tau}$ are, respectively, the spin and isospin ($1/2 \rightarrow 1/2$) transition operators and $\mathbf{S}$ and $\mathbf{T}$ those corresponding to the ($1/2 \rightarrow 3/2$) transition.

Both transition matrices consist of a spin-longitudinal and a spin-transverse component with weights depending on the Mandelstam variables s and t. For the NN $\rightarrow$ NN transition, the coefficients α and β are determined from experimental pn $\rightarrow$ np scattering data [28] and their relative weight depends on the four-momentum transfer, whereas $\gamma_{\mathrm{lo}} = \gamma_{\mathrm{tr}}$ for the NN $\rightarrow$ NΔ transition, in agreement with the experimental pN $\rightarrow$ nΔ data [40].

The Δ-N interaction potential and the ΔN $\rightarrow$ NN transition potentials are constructed in a meson exchange model [41] including π, ρ, ω and σ exchange. The Paris potential is chosen for the N-N final-state interaction.

The total cross-section consists of four amplitudes corresponding to the different physical processes described in fig. 11. Processes (a) and (b) both lead to a break-up of the deuteron into a two-proton final state. (a) is the quasi-elastic process, whereas (b) proceeds via excitation of a Δ. In both processes (c) and (d), a pion is emitted but the exit channels differ by the fact that in process (c) (coherent process), the pn system is bound as in the entrance channel, whereas it is not in process (d) (quasi-free Δ-decay). We will in the following concentrate on the inclusive and break-up processes and compare the theoretical cross-sections to the experimental yields.

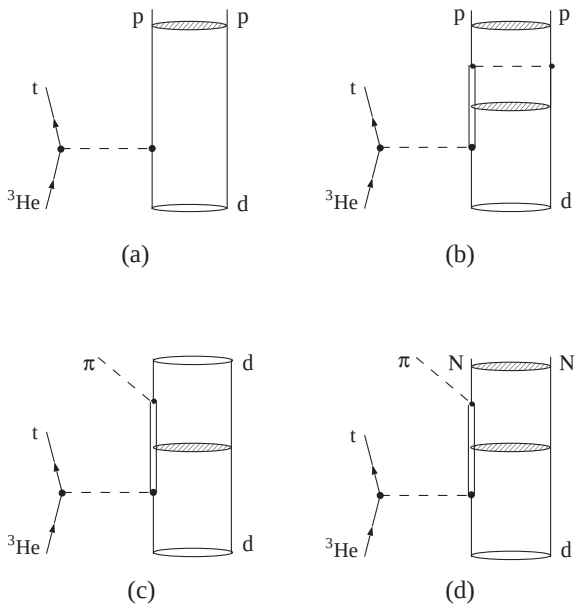

Fig. 11. Feynman diagrams for the reaction mechanisms included in the model of ref. [28]. They represent: (a) quasi-elastic scattering, (b) ΔN $\rightarrow$ NN process, (c) coherent pion production, (d) quasi-free Δ-decay. The hatched areas indicate the intermediate ΔN and NN final-state interaction.

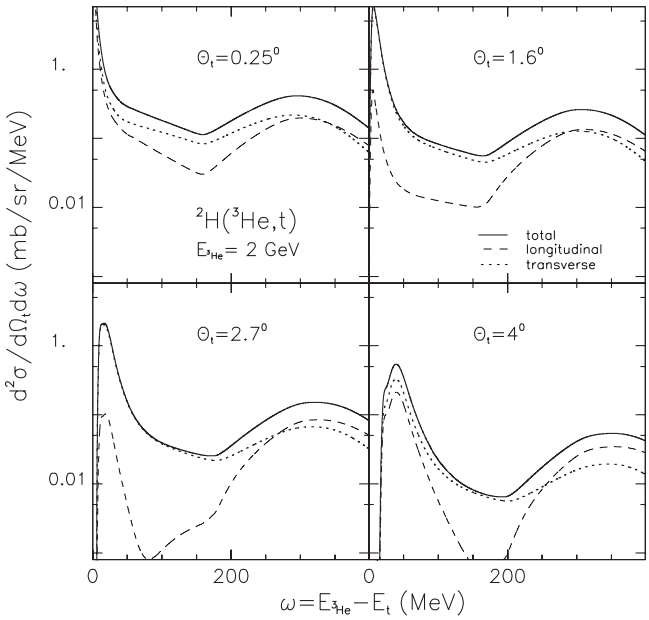

Fig. 12. Predictions of the coupled-channel model for the ^{2}H(^{3}He, t) as a function of energy transfer at four triton angles for the full interaction (solid line) and for the longitudinal (dashed lines) and transverse (dotted lines) interactions.

5.2 Theoretical results

5.2.1 ^{2}H(^{3}He, t) and ^{2}H(^{3}He, t)2p differential cross-sections

In fig. 12 and fig. 13, theoretical cross-sections for the ^{2}H(^{3}He, t) and ^{2}H(^{3}He, t)2p reactions are presented at four different angles.

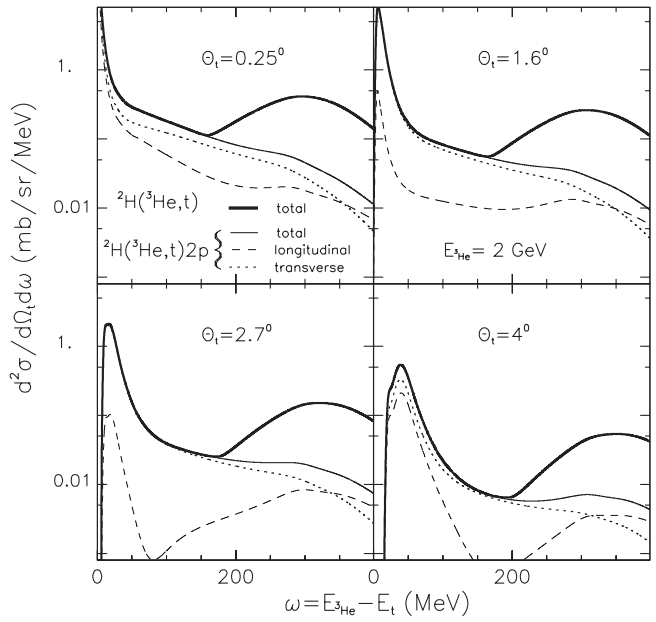

Fig. 13. Predictions of the coupled-channel model for the ^{2}H(^{3}He, t) (thick full line) and ^{2}H(^{3}He, t)2p yields (thin full line) as a function of energy transfer at four triton angles. The calculation of the ^{2}H(^{3}He, t)2p yield is shown for the longitudinal (dashed lines) and transverse (dotted lines) parts of the interaction separately.

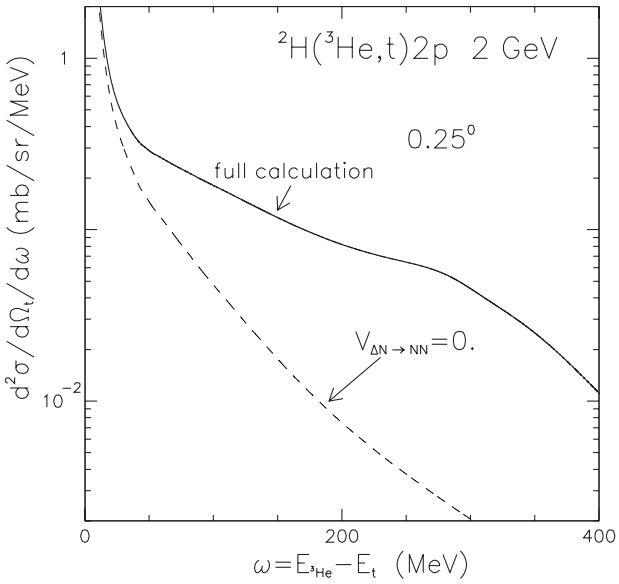

Fig. 14. Energy transfer spectrum obtained at 0.25° with the coupled-channel model for the full calculation (full line) and for the calculation with no ΔN → NN transition (dashed line).

In contrast to the inclusive reaction, the ^{2}H(^{3}He, t)2p cross-section presents no clear bump in the region of the Δ-resonance. At small angles, only a shoulder can be seen in the spectrum. At large angles, the quasi-elastic peak and the cross-section in the dip region are reduced and the presence of a structure in the ^{2}H(^{3}He, t)2p cross-section in the region of the Δ appears more clearly, although the branching ratio at the peak position stays of the order of 10% independently of the triton angle.

In order to appreciate the contribution of the Δ-resonance to the theoretical ^{2}H(^{3}He, t)2p cross-section, the result of the full calculation is compared in fig. 14 to a calculation with the ΔN → NN transition potential turned off. The effect of this transition potential is very large. It is responsible not only for the small shoulder or bump that appears in the region of the resonance peak, but also for most of the 2p yield below the pion emission threshold. This feature is due to a strong interference between the quasi-elastic process and Δ excitation followed by ΔN → NN process, which washes out completely the resonance bump. This bump appears clearly only at the largest angles, where the quasi-elastic process is reduced and the interference is smaller.

In order to study the effect of the spin structure of the interaction on the relative weights of the quasi-elastic process and Δ excitation, the calculations have been performed for the longitudinal and transverse interactions separately. The corresponding ^{2}H(^{3}He, t) and ^{2}H(^{3}He, t)2p cross-sections are plotted in fig. 12 and fig. 13.

For the inclusive ^{2}H(^{3}He, t), the relative weights of longitudinal and transverse cross-sections result, on the one hand, from the combined effects of the spin structure of the transition matrices and (^{3}He, t) form factors and, on the other hand, from the effect of the NN and ΔN interactions.

In the effective parameterization of the NN → NN transition matrix used in the model (subsect. 5.1), the transverse amplitude decreases smoothly as a function of momentum transfer. The longitudinal amplitude keeps smaller values and decreases very rapidly up to four-momentum transfers of about 150 MeV/c and then grows again smoothly. For the excitation of the Δ-resonance, the longitudinal and transverse components have an equal weight in the transition matrix, which, due to the two transverse degrees of freedom, favours the transverse cross-section by a factor 2. These features of the transition matrices are responsible for the overall evolution with the angle of both contributions and for the dominance of the transverse contribution. In particular, the very small longitudinal cross-section in the quasi-elastic peak around 2° is clearly related to the vanishing of the longitudinal amplitude in this range of momentum transfers precisely. A striking feature of these spectra is also the dominance of the transverse contribution in the dip region due to the higher interference between the quasi-elastic process and the Δ excitation for this part of the interaction. As a consequence, the predominantly transverse interference has a strong contribution up to energy transfers of about 250 MeV, washing out the resonant bump. The Δ structure is much more apparent in the longitudinal cross-section, where this interference is much smaller.

The (^{3}He, t) form-factor plays also an important role, since it reduces the cross-section when the momentum transfer increases. Due to the spin structure of ^{3}He and

t nuclei, this decrease is sharper for the transverse interaction [19], which results in an enhancement of the longitudinal yield with respect to the transverse one at the largest momentum transfers.

The Δ-N interaction enhances and shifts the Δ bump towards low energy transfers as shown in ref. [29]. It has however been shown in the case of the ^{2}H(p, n), where there are no form factors effects, that the longitudinal and transverse spectra are modified in the same manner by the Δ-N interaction, so that there is no effect on the ratio of the transverse and longitudinal contributions [42]. It has also been checked experimentally for the ^{2}H(p, n) reaction, that there is no shift between the positions of the Δ-resonance in the longitudinal and transverse channels [30,28]. In this respect, the reaction on deuterium is quite different from the reaction on a heavier nucleus. In the case of the excitation of a Δ-resonance in a carbon or lead nucleus, the residual Δ-hole interaction has indeed a large attractive effect on the longitudinal component of the interaction and a very small effect on the transverse contribution.

5.2.2 Angular distributions

The values of A_2/A_0 and A_4/A_0 ratios resulting from the fit of the theoretical angular distributions of the 2 protons in their center of mass are plotted as full lines in figs. 8 and 9 for the average angles of the experimental bins. As the quality of the fitting procedure was only checked for energy transfers larger than 100 MeV, parameters obtained below this value are not shown. The theoretical angular distributions are rather flat or slightly forward peaked (small positive A_2/A_0 and A_4/A_0 ratios), except at the largest triton angles and smallest energy transfers, where the ratios are rather high, corresponding to very forward-peaked angular distributions with a quite flat minimum, as seen in fig. 10.

This trend results from a combination of the two very different behaviours of the angular distributions induced by a longitudinal or a transverse interaction. For the two first angular bins, at energy transfers of 100 MeV, the calculated A_2/A_0 ratio is indeed negative for the transverse interaction, which means that the angular distribution has a maximum around 90°, whereas the longitudinal interaction gives high positive values, corresponding to a minimum at 90°. As a function of energy transfer, the anisotropy becomes smaller and the A_2/A_0 values obtained for both interactions converge at 400 MeV towards a same value of about 0.2. The calculated A_4/A_0 ratios keep small absolute values for both interactions at least below 300 MeV.

For the third angular bin, the trend is quite different at lower energy transfers: the transverse component (which dominates by a very large factor here) has positive A_2/A_0 and A_4/A_0 values (very forward-peaked angular distributions with a flat minimum), while the longitudinal one has a smaller A_2/A_0 ratio and a large negative A_4/A_0 ratio leading to a maximum in the angular distribution between 0° and 45°.

At small energy transfers, where the cross-section is due to the interference between the NN $\rightarrow$ NN transitions and NN $\rightarrow$ ΔN transitions followed by ΔN $\rightarrow$ NN, the angular distributions are very sensitive to the spin structure of the interaction.

At larger energy transfers, where this interference decreases and the excitation of the Δ-resonance becomes dominant, the difference between the shapes of the angular distributions induced by longitudinal and transverse interactions gets smaller, which indicates that the spin structure of the ΔN $\rightarrow$ NN transition matrix at the target excitation vertex has only a small influence on the proton angular distributions.

5.3 Discussion of pion and photoabsorption reactions on deuterium

Angular distributions of protons measured in π^+d $\rightarrow$ pp or γd $\rightarrow$ pn reactions in the region of excitation of the Δ-resonance are complementary to ^{2}H(^{3}He, t)2p, since they allow for a study of the ΔN $\rightarrow$ NN transition with, respectively, purely longitudinal and purely transverse probes.

In the case of the π^+d $\rightarrow$ pp reaction (or pp $\rightarrow$ π^+d), the angular distribution of the two protons in the center of mass has been measured for a great number of incident pion or proton energies [43] and a $1+3\cos^2\theta^*_{\rm p}$ shape ($A_2/A_0 = 1$, $A_4 = 0$) has been obtained. This result is explained mainly by the dominance of the π^+d ($^1P_2$) $\rightarrow$ ΔN ($^5S_2$) $\rightarrow$ pp ($^1D_2$) partial wave [44], but also the Δ-N interaction plays a role in the magnitude and in the shape of this differential cross-section, as was shown in different approaches [45–49].

The present coupled-channel calculation was also used to calculate observables measured in π^+d $\rightarrow$ pp and $\mathbf{p}$p $\rightarrow$ π^+d reactions. The usual πNN and πNΔ couplings were used, s-wave scattering was included and the Δ-N interaction was the same as the one used for the (^{3}He, t) calculation [42,50]. The analysing power in the $\mathbf{p}$p $\rightarrow$ π^+d reaction was correctly predicted by the model and found to be especially sensitive to the parameters of the Δ-N interaction. This result could therefore be considered as a strong test of this ingredient of the model.

The π^+d $\rightarrow$ pp differential cross-sections were also well reproduced over a large energy transfer range. In particular, center-of-mass proton angular distributions with A_2/A_0 close to 1 were predicted at the resonance. The model gives however much lower A_2/A_0 values (less forward-peaked angular distributions) for the longitudinal part of the interaction induced by the (^{3}He, t) probe at the highest energy transfers, where the Δ-resonance dominates (fig. 8). This could be due to the higher momentum transfers involved in the (^{3}He, t) reaction which might lead to higher Δ-N partial waves than the $^5S_2$ which dominates in the case of pion-induced reactions. Another difference is the presence of distortions in the (^{3}He, t) reaction. These distortions are calculated in the model in the eikonal approximation and have probably a significant effect on the $\frac{{\rm d}\sigma}{{\rm d}\Omega^*_{\rm p}}$ differential cross-sections.

In photoabsorption reactions on deuterium, angular distributions of the protons have also been measured. Due to the discernability of the emitted proton and neutron, the angular distribution has no symmetry around 90° and has also contributions from odd order Legendre polynomials, (P_1, P_3, ...) [51]. The proton angular distribution is rather flat with a maximum around 70°, which corresponds to small positive A_1/A_0 and negative A_2/A_0 values. The shape of the angular distribution of the protons is therefore quite different from the one found for pion-induced reactions. One could think that this difference is due to the different spin structure of the operators at the excitation vertex. However, the processes involved are also very different, since in the case of photon-induced reactions, besides Δ excitation, non-resonant processes like the Born term and meson exchange currents are important.

The exact shape of the proton angular distributions in γd $\rightarrow$ pp reactions could only recently be reproduced by theory by including in addition to the NN and NΔ dynamics full meson retardation in potentials and exchange currents [52].

In the (^{3}He, t) reaction, meson exchange processes might also be present. For the ^{2}H(p, n)2p experiment at 800 MeV, which differs from the previous one by the form factor only, the importance of some diagrams arising from meson exchange currents have been calculated in [53]. The interaction with a pion in flight in the transverse channel (Kroll-Ruderman term) is expected to be the largest. In the dip region, that is the region between the quasi-elastic peak and the Δ-resonance, the predicted contribution is of the same order as the Δ excitation. At the resonance peak, it should however not exceed a few percent. Such effects are therefore not expected to perceptibly modify the shape of the angular distributions in the (^{3}He, t) reaction above 250 MeV.

5.4 Comparison to ^{2}H(^{3}He, t) and ^{2}H(^{3}He, t)2p data

To allow for a direct comparison to the data, the theoretical differential cross-sections for the inclusive and 2p channels have been injected as weights in the simulation including resolution effects. Results are compared with data in fig. 7. The distortion of the theoretical curves is mainly due to the triton energy resolution (40 MeV FWHM) and to the beam angular emittance (0.3° FWHM). The latter effect is less important as the data are anyway presented by bins of 1 or 1.4 degrees. The distortion is small in the region of the Δ-resonance, where the peak is broad and where the cross-section decreases more smoothly with angle.

As expected from the studies of the high-resolution ^{2}H(^{3}He, t) data of ref. [29], the inclusive cross-section is quite well reproduced by the calculation.

The disagreement on the low-energy side of the Δ-resonance is increasing with angle. It has been discussed in detail in [29] and ascribed to Δ excitation in the projectile, which is not included in the model.

The importance of this process in the ^{2}H(^{3}He, t)2p reaction has been stressed and calculated by E. Oset *et al.* [17,32], a long time ago. In the process discussed, as a triton has to be found in the exit channel, the energy of the Δ-resonance excited in the projectile has to be carried away by a pion. The ^{2}H(^{3}He, t)2p channel is therefore free from the projectile excitation contribution, as well as from non-resonant pion production which might also have a small contribution to the inclusive yield near the pion threshold.

At energy transfers of about 150-250 MeV, where the model underestimates the inclusive cross-section, the exclusive ^{2}H(^{3}He, t)2p cross-section is well reproduced, which might confirm the contribution of projectile excitation to the inclusive spectrum.

The model gives a reasonable description of the branching ratio of the ^{2}H(^{3}He, t) reaction towards the 2p channel (fig. 7). The small value observed is in fact not surprising, considering that the π^+d $\rightarrow$ pp cross-section and γd $\rightarrow$ pn are only about 5% and 12%, respectively, of the corresponding total cross-sections at the resonance peak [44,54].

The calculation overestimates the 2p cross-section at large energy transfers and large angles. In the first angular bin, the disagreement is smaller than 30% except for the point obtained for the largest energy transfers and a renormalisation of the theoretical curve by 20% could give a good description of the data. For the larger triton angles, the overestimate gets larger in the region of the Δ-resonance peak. As the excitation of the Δ-resonance in the inclusive process is rather well described, it indicates an overestimate of the decay towards the 2p exit channel in the model.

The smooth trend of the theoretical A_2/A_0 ratio (fig. 8) is not in agreement with the values of the parameters extracted from the data which show a clear enhancement at the largest energy transfers. Although the agreement for the A_4/A_0 ratio (fig. 9) is better, the model fails in most of the cases in reproducing either the yield or the shape of the angular distributions of the protons, as illustrated in fig. 10

For energy transfers around 250 MeV, a reduction of the transverse cross-section would lead to a better agreement with the data both for the cross-section and for the A_2/A_0 ratio. However, there is no way to account for the large A_2/A_0 values at large energy transfers, since the values obtained in the model are too low for both interactions.

The relative weights of the longitudinal and transverse operators for the NN $\rightarrow$ NN and NN $\rightarrow$ NΔ transitions are fixed in the model in agreement with existing data for the n($\mathbf{p}$, $\mathbf{n}$)p or p($\mathbf{p}$, $\mathbf{n}$)Δ^{++} transitions (see subsect. 5.1). For the NN $\rightarrow$ ΔN transition, the operator consists however in principle of 16 linearly independent terms [55,56]. The three components of the $\boldsymbol{\sigma}$ operator at the projectile vertex are indeed coupled not only to the corresponding spin-longitudinal or spin-transverse components of the $\mathbf{S}_{N\rightarrow\Delta}$ operators, but also to tensor terms. In addition, non-spin-flip terms are present. The values of all the terms contributing to the NN $\rightarrow$ NΔ transition at 0° have been calculated in [56] by fitting simultaneously

the available observables of the pp $\rightarrow$ nΔ^{++} reaction and significant tensor terms have been found. Now, the form $\gamma_{\rm lo}(\boldsymbol{\sigma}\cdot\mathbf{q})(\mathbf{S}^{\dagger}\cdot\mathbf{q})+\gamma_{\rm tr}(\boldsymbol{\sigma}\times\mathbf{q})(\mathbf{S}^{\dagger}\times\mathbf{q})$ for the NN $\rightarrow$ ΔN transition matrix which is taken for the sake of simplicity allows for a satisfactory agreement of the p($\mathbf{p}$, $\mathbf{n}$) spin observables, with $\gamma_{\rm lo}=\gamma_{\rm tr}$. However, with such an interaction, the angular distributions of the pions resulting from the decay of the Δ-resonance in the reactions pp $\rightarrow$ nΔ^{++} and ^{3}He+p $\rightarrow$ tΔ^{++} could not be reproduced [57]. This has been attributed by the author to tensor terms in the excitation of the Δ at the target vertex.

The angular distributions of pions in the Δ frame could indeed be more sensitive to the form of the operator of the N $\rightarrow$ Δ transition than the ($\mathbf{p}$, $\mathbf{n}$) spin observables which measure only the weights of the $(\boldsymbol{\sigma}\cdot\mathbf{q})$ and $(\boldsymbol{\sigma}\times\mathbf{q})$ terms related to the NN vertex.

The influence of such tensor terms in the N $\rightarrow$ Δ transition on the cross-sections and proton angular distributions in the reaction ^{2}H(^{3}He, t)2p is not known. Nevertheless, as the interaction of ref. [56] seems to provide a better description of the bulk of existing data, especially those linked with the Δ de-excitation vertex, a calculation of the ^{2}H(^{3}He, t)2p cross-sections and proton angular distributions with this interaction should be very interesting.

The disagreement between the present calculation and data might also have other sources. By modifying the momentum transfer direction, the projectile distortions have probably a sizeable effect on the proton angular distributions. The eikonal approximation used in the calculation might not be sufficient to deal with these distortions. Another important ingredient of the calculation is the Δ-N interaction and the ΔN $\rightarrow$ NN transition potential. As explained in sect. 3, the parameters have been validated by a comparison of the coupled-channel calculations to the existing $\mathbf{p}$p $\rightarrow$ dπ^+ data. The kinematics are however different in the case of (^{3}He, t) and it could be worth investigating the sensitivity of the cross-sections and angular distributions to the interaction.

6 Conclusion

Data obtained in the ^{2}H(^{3}He, t)2p reaction at 2 GeV have been presented. A careful study of the acceptance corrections and resolution effects has been necessary in order to analyse the data. The energy transfer spectra extend well above the pion threshold, but the cross-section of the ^{2}H(^{3}He, t)2p reaction in the region of the Δ-resonance is less than 10% of the inclusive cross-section. This indicates the small branching ratio of the ΔN $\rightarrow$ NN process with respect to the other Δ-decay channels.

The distribution of the proton angles measured with respect to the momentum transfer direction in the two-proton center of mass has been analysed as a function of energy transfer and triton angle. The evolution of the shapes of the angular distributions has been studied by means of a Legendre polynomials combination fit. These results are complementary to the ones obtained in pion and photoabsorption on deuterium and offer a good basis to test models.

The data have been compared to predictions of a coupled-channel model including NN and ΔN intermediate states for the description of the ^{2}H(^{3}He, t) and ^{2}H(^{3}He, t)2p reactions. This model reproduces the gross features of the ^{2}H(^{3}He, t)2p energy transfer spectra.

Up to energy transfers of about 250 MeV, the yield of the ^{2}H(^{3}He, t)2p reaction is mainly due to spin-transverse excitation, where a strong interference between the quasi-elastic process and Δ excitation arises and smears out the resonant structure of the Δ-resonance. In this region, the cross-section is well reproduced, in contrast with the inclusive ^{2}H(^{3}He, t) data or with the transverse component in the ^{2}H($\mathbf{p}$, $\mathbf{n}$) reaction [28]. This last result indicates a small contribution of meson exchange currents and confirms the interpretation of the observed excess of cross-section by projectile excitation.

The model overestimates the cross-section at energy transfers larger than 250 MeV, which indicates that the theoretical branching ratio of the Δ-resonance towards ΔN $\rightarrow$ NN seems to be too large in this energy transfer range. A study of the sensitivity of the branching ratio to this parameter might be interesting to understand the origin of this deviation.

In addition, the anisotropies of the angular distributions are not well reproduced by the model. The shapes of the theoretical angular distributions are very sensitive to the spin structure (longitudinal or transverse) of the excitation, especially below 300 MeV and the simple form used for the transition operator at the N $\rightarrow$ Δ vertex might not be adequate. A comparison with a model including a more general interaction as [56] would be most helpful to clarify this point. Measurements of proton angular distributions for longitudinal and transverse channels separately in the ^{2}H($\mathbf{p}$, $\mathbf{n}$)2p reaction could bring valuable additional information to this discussion and help to disentangle effects in the proton angular distributions related to the excitation vertex and to the Δ-N interaction and ΔN $\rightarrow$ NN process.

We gratefully acknowledge the support from the technical staff at Laboratoire National Saturne. We wish to thank B. Lucas and A. Le Merdy for their help in the initial stage of the experiment. We gratefully acknowledge G. Chesneau, R. Margaria and R. Skowron for their efficient technical assistance. We took benefit of very fruitful discussions with C. Wilkin, E. Oset and A. Deloff during the course of this work. We are very grateful to them. This work has been supported in part by IN2P3 of CNRS, by DSM of CEA, by the Danish and Swedish National Research Councils, by the Carlsberg Foundation and by the Polish State Committee for scientific research under grant 2 P 302 04604.

References

1. C. Ellegaard *et al.*, Phys. Rev. Lett. **50**, 1745 (1983).
2. C. Ellegaard *et al.*, Phys. Lett. B **154**, 110 (1985).
3. D. Contardo *et al.*, Phys. Lett. B **168**, 331 (1986).
4. T. Hennino *et al.*, Phys. Lett. B **283**, 42 (1992).
5. T. Hennino *et al.*, Phys. Lett. B **303**, 236 (1993).

6. S. Tarlé-Rousteau, *Etude des voies de décroissance de la résonance Δ excitée dans l' ^{4}He et autres noyaux par la réaction (^{3}He, t) à 2 GeV.*, Thèse, Université Joseph Fourier, Grenoble, France, 1995.
7. M. Österlund, *Experimental Studies of Delta Excitations in Nuclei, Using the (d, ^{2}He) and (^{3}He, t) Reactions*, Comprehensive Summaries of Uppsala Dissertations from the Faculty of Science and Technology 628 (2001), ISBN 91-554-5024-5.
8. V.N. Baturin *et al.*, Sov. J. Nucl. Phys. Preprint LNPHI **31**, 207 (1980).
9. D.A. Lind, Can. J. Phys. **65**, 637 (1987).
10. D. Prout *et al.*, Phys. Rev. Lett. **76**, 4488 (1996).
11. J. Chiba *et al.*, Phys. Rev. Lett. **67**, 1982 (1991).
12. C. Ellegaard *et al.*, Phys. Lett. B **231**, 365 (1989).
13. V.G. Ableev *et al.*, JETP Lett. **40**, 763 (1984).
14. S. Avramenko *et al.*, Nucl. Phys. A **596**, 355 (1996).
15. M. Roy-Stephan, Nucl. Phys. A **488**, 187c (1988).
16. C. Gaarde, Annu. Rev. Nucl. Part. Sci. **41**, 187 (1991).
17. E. Oset, E. Shiino, H. Toki, Phys. Lett. B **224**, 249 (1989).
18. T. Udagawa, S.W. Hong, F. Osterfeld, Phys. Lett. B **245**, 1 (1990).
19. J. Delorme, P.A.M. Guichon, Phys. Lett. B **263**, 157 (1991).
20. P.F. de Cordoba, J. Nieves, E. Oset, M. Vicente-Vacas, Phys. Lett B **319**, 416 (1993).
21. T. Udagawa, P. Oltmanns, F. Osterfeld, S. Hong, Phys. Rev. C **49**, 3162 (1994).
22. M.A. Kagarlis, V.F. Dmitriev, Phys. Lett. B **408**, 12 (1997).
23. G. Chanfray, M. Ericson, Phys. Lett. B **141**, 163 (1984).
24. V.F. Dmitriev, T. Suzuki, Nucl. Phys. A **438**, 697 (1985).
25. T. Taddeucci *et al.*, Phys. Rev. Lett. **73**, 3516 (1994).
26. Y. Nakaoka, M. Ichimura, Prog. Theor. Phys. **102**, 599 (1999).
27. Y. Jo, C.Y. Lee, Phys. Rev. C **54**, 952 (1996).
28. C. Mosbacher, F. Osterfeld, Phys. Rev. C **56**, 2014 (1997).
29. B. Ramstein *et al.*, Eur. Phys. J. A **6**, 225 (1999).
30. D. Prout *et al.*, Nucl. Phys. A **577**, 233c (1994).
31. S. Boffi, C. Giusti, F.D. Pacati, Phys. Rep. **226**, 1 (1993).
32. E. Oset, P.F. de Cordoba, J. Nieves, M.J.V. Vacas, Phys. Scr. **48**, 101 (1993).
33. B.S. Aladashvili *et al.*, J. Phys. G **3**, 1225 (1977).
34. A. Deloff, T. Siemiarczuk, Nucl. Phys. A **555**, 659 (1993).
35. C. Comptour *et al.*, Nucl. Phys. A **579**, 369 (1994).
36. J.P. Alard *et al.*, Nucl. Instrum. Methods A **261**, 379 (1987).
37. K. Bouyakhlef, *Etude experimentale de l'interaction proton-proton a $T_{\rm inc} = 0.8$ et 2.5 GeV avec le détecteur DIOGENE. Test du détecteur*, Thèse de l'Université de Clermont II, 1990.
38. M. Stampe, *One and two proton emission following the (^{3}He, t) reaction at 2 GeV*, Master Thesis, Niels Bohr Institute, 1996.
39. C. Ellegaard *et al.*, Phys. Rev. Lett. **59**, 974 (1987).
40. G. Glass *et al.*, Phys. Lett. **129**, 27 (1983).
41. R. Machleidt, K. Holinde, C. Elster, Phys. Rep. **149**, 1 (1987).
42. C. Mosbacher, *Hadronische Reaktionen am Deuteron im Δ-Resonanzbereich,* Thesis, Institut für Kernphysik, Forschungszentrum Jülich, Friedrich-Wilhelms-Universität Bonn, 1998.
43. J. Hoftiezer *et al.*, Nucl. Phys. A **402**, 429 (1983).
44. T. Ericson, W. Weise, *Pions and Nuclei* (Clarendon, Oxford, 1988).
45. J.A. Niskanen, Nucl. Phys. A **298**, 417 (1978).
46. O. Maxwell, W. Weise, M. Brack, Nucl. Phys. A **348**, 388 (1980).
47. B. Blankleider, I. Afnan, Phys. Rev. C **24**, 1572 (1981).
48. H. Pöpping, P. Sauer, Z. Xi-Zhen, Nucl. Phys. A **474**, 557 (1987).
49. M. Peña, H. Garcilazo, U. Oelfke, P. Sauer, Phys. Rev. C **45**, 1487 (1992).
50. C. Mosbacher, F. Osterfeld, Acta Phys. Pol. B **29**, 3087 (1998).
51. R. Crawford *et al.*, Nucl. Phys. A **603**, 303 (1996).
52. M. Schwamb, H. Arenhövel, P. Wilhelm, T. Wilbois, Phys. Lett. B **420**, 255 (1998).
53. C.A. Mosbacher, *Mesonaustauschströme in (p, n)-reaktionen am deuterium,* Diplomarbeit, Institut für Kernphysik, Forschungszentrum Jülich, Friedrich-Wilhelms-Universität Bonn, 1995.
54. J. Arends *et al.*, Nucl. Phys. A **412**, 509 (1984).
55. J. Auger, C. Lazard, R.J. Lombard, R. Silbar, Nucl. Phys. A **442**, 621 (1985).
56. L. Ray, Phys. Rev. C **49**, 2109 (1994).
57. R. Dahl, *Angular correlations in Δ decay,* Master Thesis, Niels Bohr Institute, 1995.